Applied Mechanics and Materials Vols. 373-375 (2013) pp 265-270
© (2013) Trans Tech Publications, Switzerland
doi:10.4028/www.scientific.net/AMM.373-375.265

Design and Kinematics Analysis of Propulsion Mechanism of Biped Robot Running on Water

Xu Linsen[1, a], Wei Xianming[2, b], Cao Kai[2, c], Luo Mingzhou[1, d] and Shiyungao[2, e]

[1]Hefei Institutes of Physical Science, Chinese Academy of Science, Hefei, 230031, China

[2] Changzhou Institute of Advanced Manufacturing Technology, Changzhou, 213164, China

[a]lsxu@iamt.ac.cn, [b]xmwei@iamt.ac.cn, [c]kcao@iamt.ac.cn, [d]lmz@iim.ac.cn, [e]ygshi@iamt.ac.cn

Keywords: Biped Robot; Running on Water; Design and Dynamics Analysis; Propulsion Mechanism

Abstract. A biped robot is designed to simulate the water running function of the basilisk lizard. The propulsion mechanism and the control system of the robot are studied. Based on the water running process of the lizard, the changed Watt-I planar linkages are developed to provide the lifting and propulsion forces to run on water. On the basis of the movement equations of the four-bar mechanism and the coordinate transformation equations, the double bar Assur Group movement trajectories of the linkages are deduced to simulate the foot trajectories of the lizard. According to the kinematics principle of the planar four-bar linkage, we have studied the kinematics parameters of the Watt-I linkage, which are the basis of the manufacturing of the prototype. The real prototype of the robot is manufactured to test its function of water running. The lifting and propulsion force generated by the mechanism is similar with the basilisk lizard, whose value is about 1.3N. The experiment results show that the propulsion mechanism can satisfy the requirement of biped robot running on water.

Introduction

The requirement that the robot has the functions of walking on both land and water is brought out to implement the works such as military surveillance, water quality monitoring, wetland detection, search and rescue in the complex environments. The technologies of the legged robot walking on the hard land surface are mature relatively[1-2], so it has been the research hotspot in the robotics that studying the mechanisms of the legged robot walking on the different kinds of material surface such as water and soft sand to expand its walk domain.

Yun Seong Song etc. has developed a robot with twelve legs which can walk on water by mimicking the water skipper[3]. The robot floats by use of the water surface tension and moves by driving the special paddle-type legs, so the payload of the robot is low (9.3g) and its walk velocity is slow (3cm/s). Steven Floyd etc. has developed a quadruped robot walking on water, which realizes the water walk function by its four disk feet striking water[4]. The robot feet move with the constant angles, which lead to the bigger resistance when they are lifted and reduces the robot's payload (50g).

The basilisk lizard is capable of walking across the surface of water at approximately 1.5 m/s, and a stepping rate of 5-10Hz (per leg). Compared with a ship, the lizard's move mode leads to the smaller volume under water and can reduce the water resistance, which can promote the propeller efficiency. Compared with the quadruped water running method, the biped method is to the benefit of the robot energy saving and balance keeping, and the biped robot gait is simple to control.

In this case, we first emulate the water walking function of the lizard by a Watt-I six-bar linkage, and the propulsion mechanism is developed. Then the kinematics analysis on the robot is implemented to select the driver motor and the material of the robot body.

Research on Dynamic Mechanism of Biped Robot Walking on Water

A basilisk's water walking stride can be roughly divided into three phases: slap, stroke and recovery. The forces experienced by the leg and foot are different in each phase, and have differing effects on the lizard's ability to stay afloat. These phases are shown in Fig. 1. Surface tension effects

on the ability to run on the water's surface are negligible. The trajectories of the knee, the ankle and the sole in one leg of the lizard can be considered in a plane approximately, which are shown in Fig.2.

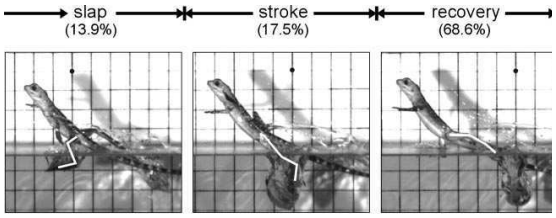

Fig.1 Pictures of a basilisk lizard walking on water

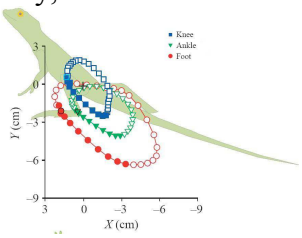

Fig.2 Movement trajectories of a basilisk lizard walking on water

We implement the water walking function of the biped robot by simulating the gait and the sole trajectory of the lizard walking on water. Because the forces experienced by the leg and foot in the slap phase and the recovery phase are negligible compared with the force in the stroke phase, the lifting and propulsion force in the stroke phase are mainly taken into account. In the stroke phase, the lizard pushes against the water beneath its foot, stroking downward and creating an air cavity in the water. The momentum transfer from the lizard's foot to the water during this stroke phase generates the main lifting and propulsion force. The force for a lizard's foot entering the water is[5]:

$$F_{str}(t) = C_D^*[0.5S\rho \cdot v^2 + S\rho \cdot gh(t)], \tag{1}$$

where $C_D^* \approx 0.703$ is the constant drag coefficient, ρ is the density of water, g is the acceleration due to gravity, S is the area over which drag is occurring, and $h(t)$ is the time varying depth of the foot. This holds true over a large range of velocities for both lizards and experimental equipment. The force curve in a stride can be got according to the above equation, which is shown as Fig.3.

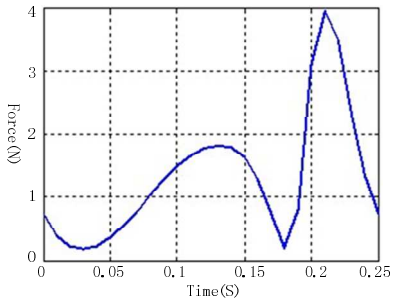

Fig.3 Force curve in the simulation environment

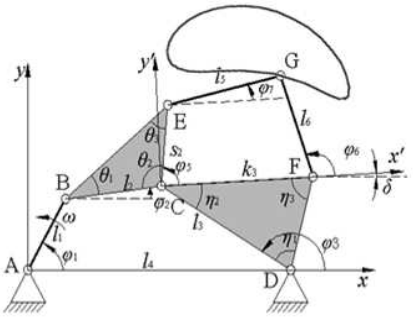

Fig.4 Watt-I planar linkage

Design of the propulsion mechanism

2.1 Kinematics analysis of the double bar Assur Group of Watt-I linkage

Watt-I linkage is shown as Fig.4. The link rods of *AB*, *BC*, *CD* and *AD* constitute the grounded four-bar linkage, whose lengths are represented by l_1, l_2, l_3 and l_4 respectively. Suppose that the angles between the rods *AB*, *BC*, *CD* and the *x*-axis are φ_1, φ_2, φ_3 respectively, and the interior angles of ΔBCE and ΔDCF are θ_i and φ_i (i=1, 2, 3) respectively. The rod *AB* is the driving rod with a constant angular velocity of ω. So the angular displacements can be known as following respectively[6]:

$$\begin{cases} \varphi_3 = 2\tan^{-1}\dfrac{N+\sqrt{M^2+N^2-Q^2}}{M-Q} \\ \varphi_2 = \tan^{-1}\dfrac{N+l_3\sin\varphi_3}{M+l_3\cos\varphi_3} \end{cases}, \tag{2}$$

where $M = l_4 - l_1\cos\varphi_1$, $N = -l_1\sin\varphi_1$, $Q = \dfrac{M^2+N^2+l_3^2-l_2^2}{2l_3}$ and $\varphi_1 = \omega t$。

And the trajectory of the point *C* can be got from Eq. 2:

$$\begin{pmatrix} x_C \\ y_C \end{pmatrix} = \begin{pmatrix} l_1 \cos\varphi_1 + l_2 \cos\varphi_2 \\ l_1 \sin\varphi_1 + l_2 \sin\varphi_2 \end{pmatrix}. \tag{3}$$

The mechanism of *ABCD* is a quadrilateral, so

$$\angle BCD = \varphi_3 - \varphi_2 . \tag{4}$$

Supposing that $\angle ECF = \varphi_5$, its value can be deduced out from Eq. 4:

$$\varphi_5 = 2\pi - \theta_2 - \eta_2 - (\varphi_3 - \varphi_2) . \tag{5}$$

A new coordinate system *x*'*Cy*' is built by setting the point *C* as the origin and side *CF* as the *x*'-axis, and the angle between the *x*'-axis and the *x*-axis is got as:

$$\delta = \varphi_3 - \eta_3 - \eta_1 . \tag{6}$$

The link rods of *CE*, *EG*, *GF* and *CF* constitute a four-bar linkage also, and the lengths are represented as s_2, l_5, l_6 and k_3 respectively. The rod *CE* is looked as the driving rod. And suppose the angles between the rods *EG*, *FG* and the *x*'-axis are φ_7 and φ_6 respectively:

$$\begin{cases} \varphi_6 = 2\tan^{-1}\dfrac{J + \sqrt{H^2 + J^2 - K^2}}{H - K} \\ \varphi_7 = \tan^{-1}\dfrac{J + l_6 \sin\varphi_6}{H + l_6 \cos\varphi_6} \end{cases}, \tag{7}$$

where $H = k_3 - s_2 \cos\varphi_5$, $J = -s_2 \sin\varphi_5$, $K = \dfrac{H^2 + J^2 + l_6^2 - l_5^2}{2l_6}$.

So the trajectory of the point *G* in the coordinate system *x*'C*y*' can be deduced:

$$\begin{pmatrix} x_G^{'} \\ y_G^{'} \end{pmatrix} = \begin{pmatrix} s_2 \cos\varphi_5 + l_5 \cos\varphi_7 \\ s_2 \sin\varphi_5 + l_5 \sin\varphi_7 \end{pmatrix}. \tag{8}$$

And the trajectory of the point *G* in the coordinate system *x*A*y* can be got according to the transformation formulas of the coordinates:

$$\begin{pmatrix} x_G \\ y_G \end{pmatrix} = \begin{pmatrix} x_G^{'} \cos\delta - y_G^{'} \sin\delta + x_C \\ y_G^{'} \sin\delta + y_G^{'} \cos\delta + y_C \end{pmatrix}. \tag{9}$$

The trajectory of the point *G* is shown as Fig.4.

2.2 Design of the virtual prototype of the propulsion mechanism

The trajectory of the point *G* shown in Fig.4 is similar with the sole trajectory of the basilisk lizard shown in Fig.2, so we adopt the improved Watt-I mechanism as the lifting and propulsion mechanism of the biped robot.

We look the point *G* as the center point of the robot's sole, and move it to be under the *x*-axis to implement the stroke function of the lifting and propulsion mechanism. Simultaneously the triangle plates are replaced by the slender rods. So $\theta_1=\pi$ and $\eta_1=0$, and from the above equations we can get as follows: $\theta_2=\theta_3=\eta_2=0$, $\eta_3=\pi$ and

$$\begin{cases} \varphi_5 = 2\pi - \varphi_3 + \varphi_2 \\ \delta = \varphi_3 - \pi \end{cases}. \tag{10}$$

Moreover, we rotate the rod *AD* an angle less than $\pi/4$ around point *A* to make the sole parallel to the water surface, then the lifting and propulsion force may be bigger, which is shown as Fig.5.

It can be known from Fig.1 that the two feet slap the water surface alternately during the lizard walking on water. So we design the same propulsion mechanisms for the both sides of the robot. The mechanisms are driven by a same motor, but their phase difference is π, which is shown as Fig. 6.

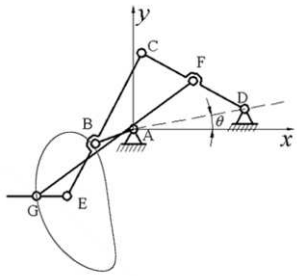

Fig.5 Skeleton of the robot propulsion mechanism

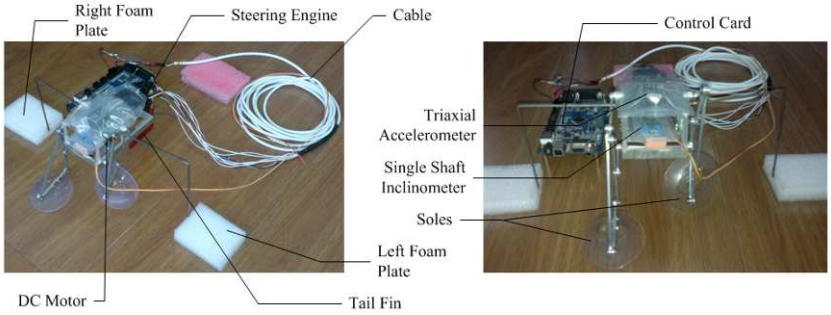

Fig.6 Prototype of the biped robot walking on water

Kinematics analysis on the biped robot

The angular velocities of the link rods *CD* and *BC* can be deduced as follows respectively by the kinematics principle of the four-bar linkage:

$$\left.\begin{aligned}\omega_3 &= \omega\frac{l_1\sin(\varphi_1-\varphi_2)}{l_3\sin(\varphi_3-\varphi_2)}\\ \omega_2 &= -\omega\frac{l_1\sin(\varphi_1-\varphi_3)}{l_2\sin(\varphi_2-\varphi_3)}\end{aligned}\right\}, \tag{11}$$

and whose angular accelerations are respectively:

$$\left.\begin{aligned}\alpha_3 &= \frac{l_2\omega_2^2+l_1\omega_1^2\cos(\varphi_1-\varphi_2)-l_3\omega_3^2\cos(\varphi_3-\varphi_2)}{l_3\sin(\varphi_3-\varphi_2)}\\ \alpha_2 &= \frac{l_3\omega_3^2-l_1\omega_1^2\cos(\varphi_1-\varphi_3)-l_2\omega_2^2\cos(\varphi_2-\varphi_3)}{l_2\sin(\varphi_2-\varphi_3)}\end{aligned}\right\}. \tag{12}$$

It can be known from Eq.10 that the angular velocity and acceleration of φ_5 are as follows respectively:

$$\left.\begin{aligned}\omega_5 &= \text{-}\omega_3+\omega_2\\ \alpha_5 &= -\alpha_3+\alpha_2\end{aligned}\right\}. \tag{13}$$

Similarly, the angular velocity and acceleration of δ are as follows respectively:

$$\left.\begin{aligned}\omega_\delta &= \omega_3\\ \alpha_\delta &= \alpha_3\end{aligned}\right\} \tag{14}$$

The angular velocities and accelerations of the link rods of *GF* and *EG* in the coordinate system *x'Cy'* are respectively:

$$\left.\begin{aligned}\omega_6' &= \omega_5\frac{s_2\sin(\varphi_5-\varphi_7)}{l_6\sin(\varphi_6-\varphi_7)}\\ \omega_7' &= -\omega_5\frac{s_2\sin(\varphi_5-\varphi_6)}{l_5\sin(\varphi_7-\varphi_6)}\end{aligned}\right\}, \tag{15}$$

$$\left.\begin{aligned}\alpha_6' &= \frac{l_5\omega_7'^2+s_2\omega_5'^2\cos(\varphi_5-\varphi_7)-l_6\omega_6'^2\cos(\varphi_6-\varphi_7)}{l_6\sin(\varphi_6-\varphi_7)}\\ \alpha_7' &= \frac{l_6\omega_6'^2-s_2\omega_5'^2\cos(\varphi_5-\varphi_6)-l_5\omega_7'^2\cos(\varphi_7-\varphi_6)}{l_5\sin(\varphi_7-\varphi_6)}\end{aligned}\right\}. \tag{16}$$

It can be got that the angular velocities and accelerations of the link rods of *GF* and *EG* in the coordinate system *xAy* are as follows:

$$\left.\begin{aligned}\omega_6 &= \omega_3 + \omega_6' \\ \omega_7 &= \omega_3 + \omega_7'\end{aligned}\right\}, \tag{17}$$

$$\left.\begin{aligned}\alpha_6 &= \alpha_3 + \alpha_6' \\ \alpha_7 &= \alpha_3 + \alpha_7'\end{aligned}\right\}. \tag{18}$$

Experiments

4.1 Manufacture of the biped robot prototype

In consideration of the functional requirement of the biped robot running on water, the main body frame and the propulsion mechanism must be light enough. So we take the aluminium alloy LY12 as the material of the main body frame and the propulsion mechanism. We take the drive module MAXON 221011+134161 as the drive system of the robot, whose rated power is 5W and rated torque is 0.15 Nm. And we take the flexible rubber to make the robot feet. The prototype of the biped robot is shown as Fig.7, whose total weight is 3.2N.

4.2 Experiments of the biped robot prototype

The volumes of the left foam plate and the right one are 91.605cm³ and 97.712 cm³ respectively, and the total buoyancy of the two foam plates is 1.856N when they are all under water. The buoyancy is less than its gravity, so the robot will sink when it is placed on the water surface statically.

The sequence diagrams of the robot working on water are shown as Fig. 7. The robot can walk on water due to the force produced by the legs slapping from 1s to 4s. If we cut off the power supply when the time is 4s, then the robot will stop slapping and begin to sink.

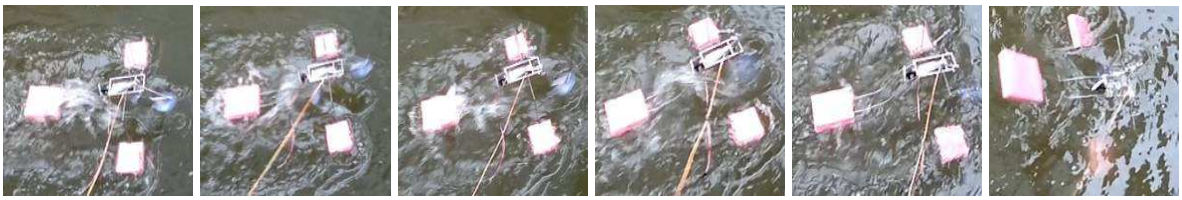

Fig. 7 Sequence diagrams of the robot walking on water

It can be known from Fig. 7 that the lifting force produced by the legs is the main factor to keep the robot away from sinking.

4.3 Measurement of the lifting and propulsion force

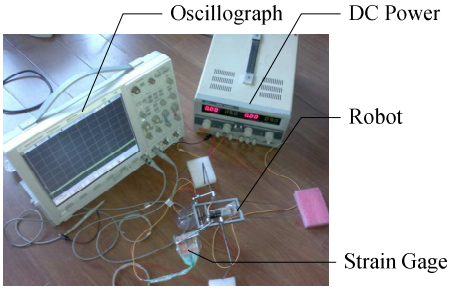

Fig. 8 Experimental platform

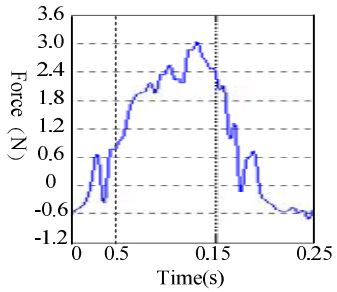

Fig.9 Force curve measured by the strain gauge

The force is the decisive factor of the robot's load capacity, that is, the force is larger, its load capacity is stronger. We build an experimental platform shown as Fig. 8 to test the lifting and propulsion force of the robot. We mount the strain gages on both soles, and the voltage variation of one of the strain gages is shown by an oscillograph, from which the lifting and propulsion force can be got. And the curve of the lifting and propulsion force is shown as Fig. 9.

The force curve in Fig. 9 is similar to the curve in the simulation environment shown as Fig.3. The maximum value of the lifting and propulsion force in Fig.3 is 3.6N, which is less than the force value of 4N in the simulation environment. The simulation force values are bigger than the realistic ones because that the transmission efficiency, the pressure of the atmosphere and the deformation of the soles are not considered in the simulating process. In the reality environment, the reaction force during the recovery phase from water is opposite the force during the slap and stroke phase, so there are negative points in the curve of Fig.9.

Conclusions

The function of the biped robot walking on water are studied in this paper, which will offer theoretical and design basis for developing the bionic amphibious biped robot, and the next work will be as follows:

① The model of the amphibious biped robot will be built to promote the movement flexibility and environmental adaptability of the robot as the amphibians;

② The composite propulsion mechanism of the amphibious biped robot will be designed, and the propulsion movement on land and water will be implemented by using the different modes of motion and control of the mechanism;

③ The motion control method of the amphibious biped mechanism will be studied to implement the control method of the robot motion mode such as going straight, turning and avoiding obstacle.

Acknowledgments

This work is supported by the National Natural Science Foundation of China (No. 50905175), and the National Program on Key Basic Research Project of China (No. 2011CB302106).

References

[1] Gao Feng. Reflection on the Current Status and Development Strategy of Mechanism Research[J]. Chinese Journal of Mechanical Engineering, vol. 41, no. 8, 2005, pp: 3-17.(In Chinese).

[2] DONG Xiao-po, Wang Xu-ben. Development of Rescue Robot Technology and Its Application in Disaster[J]. Journal of Disaster Prevention and Mitigation Engineering, vol. 27, no. 1, 2007, pp: 112-117. (In Chinese)

[3] Song Yun Seong, Sitti Metin. Surface-tension -driven biologically inspired water strider robots: Theory and experiments [J]. IEEE Transactions on Robotics, vol. 23, no. 3, 2007, pp: 578-589.

[4] Floyd Steven; Sitti Metin. Design and Development of the Lifting and Propulsion Mechanism for a Biologically Inspired Water Runner Robot[J]. IEEE transactions on robotics, vol. 24, no 3, 2008, pp: 698-709.

[5] T. Hsieh and G Lauder. Running on water: Three-dimensional force generation by basilisk lizards [J]. PNAS, vol. 101, 2004, pp: 16784-16788.

[6] Zhen Wenwei, Wu Kejian. MECHANISMS AND MACHINE THEORY[M]. 5th ed. Beijing: High Education Press, 1997. (In Chinese)

[7] Linsen Xu, Bing Li, Feng Xu, Jianghai Zhao, and Baolin Feng. Optimization Synthesis on Water Running Mechanism of Biped Robot [J]. Advanced Materials Research, Vol. 211-212, 2011, pp: 454-459.

[8] J.A. Mirth, T.R. Chase. Circuits and branches of single-degree-of freedom planar linkages [J]. ASME Journal of Mechanical Design, vol. 115, 1993, pp: 223–230.

[9] Linsen Xu, Kai Cao, Xianming Wei, Yungao Shi. Dynamic Analysis of Fluid-Structure Interaction for the Biped Robot Running on Water[C]. The 12th International Conference on Control, Automation, Robotics and Vision, 5-7th December 2012, Guangzhou, China, pp: 1546-1550.